Preprints of the 21st IFAC World Congress (Virtual)
Berlin, Germany, July 12-17, 2020

Coordinated Control for Combined Heat and Power Load of an Integrated Energy System

Yuhui Jin*, Junli Zhang*, Xiao Wu*, Jiong Shen*, Kwang Y. Lee**

** Key Laboratory of Energy Thermal Conversion and Control of Ministry of Education, School of Energy and Environment, Southeast University, Nanjing, 210096, China (e-mail: yuhuijin@seu.edu.cn; zjli@seu.edu.cn; wux@seu.edu.cn; Corresponding author: shenj@seu.edu.cn)*
*** Department of Electrical and Computer Engineering, Baylor University, One Bear Place #97356, Waco, TX 76798-7356, USA (e-mail: Kwang_Y_Lee@baylor.edu)*

Abstract: Most stand-alone integrated energy systems (IES) with renewable energy can only meet the demand of electrical load, not both electrical load and thermal load. Those studies on combined heat and power cogeneration systems mainly focus on the optimal scheduling of each source, ignoring the difference in dynamic response between electrical and thermal processes. In fact, the different response speeds of electrical and thermal objects will bring in challenges to control. In order to specify and solve the issue, this paper proposes a detailed mechanism model of a standard IES. A model predictive control (MPC) controller is designed and tuned based on the state-space form of the system. The control simulation results imply the feasibility of the MPC controller in coordinating both electricity and heat.

Keywords: Integrated energy system, Stand-alone, Coordinated control, Combined heat and power generation, Model predictive control

1. INTRODUCTION

Energy consumption is a key index of national development. With the ever increasing concerns about environment, conventional fossil fuels such as coal and petroleum no longer meet the demand of sustainability. On the contrary, renewable energy sources have abundant reserves and produces negligible emissions. Even though the technology development and government polices both encourage the application of renewable energy, the conditioned ability of the large power grid still impede a higher proportional embrace of renewable energy. Therefore, stand-alone or distributed generation (DG) systems stand out and become the mainstream form of renewable energy consumption.

Because of the advantages such as small capacity and flexibility, stand-alone integrated energy systems (IES) are suitable for localized domestic energy supply. The energy used for heating and hot water takes large part of the whole domestic energy consumption. For example, the proportion of heating reaches 23.0% of the total building energy consumption in urban northern China, while hot water in China's urban areas accounts for 23.4% of the total residential building energy consumption in 2008. Therefore, combined heat and power (CHP) cogeneration IES has arose much attention in recent years. However, most literatures about the energy management of IES mainly focused on the energy balance in electricity supply, regardless of the thermal one. The proposed study will go a step further to take the dynamic characteristics of thermal processes into account.

The most commonly used approach of managing the energy supply of IES is optimal scheduling. The devices of IES receive the set-point instructions and operate under set-point tracking mode. For instance, Das (Das and Al-Abdeli, 2017) studied the role of both electric and heating loads on the optimization of hybrid stand-alone CHP systems. Zhang (Zhang et al., 2019) proposed a stochastic model predictive control framework to optimally schedule the CHP micro-grid. In this way, the zero-offset energy balance of the system relies strongly on fast-response of stable sources, such as batteries. However, the relatively high investment cost and short life span limit the installation capacity of batteries. Without the support of batteries, stand-alone micro grid is unable to keep good balance between the power supply and load demand.

In this paper, an energy balance based direct control method is proposed to coordinate a CHP micro grid IES. Without upper layer optimization, the control variables are directly decided by the real time energy supply and demand. Every component of the system will operate together to balance the energy. Therefore, the dependency of reliable, fast-response sources can be mitigated. Nonetheless, the combination of renewable energy sources and CHP may bring in great challenges to dynamic control. The challenge mainly derives from the intermittency of the renewable sources and the considerable difference between the dynamic characteristics of electrical and thermal processes. In short, the response time of electrical components is much shorter than that of the thermal components.

Copyright lies with the authors

The remaining of the study is as follow: Modelling of a standard renewable energy powered stand-alone IES is established in Section 2. In Section 3, an MPC controller is designed according to the systematic dynamic characteristics, for the purpose of coordinating each component for energy balance. In Section 4, the performance of control simulation suggests the potential feasibility of MPC controllers. Finally, conclusions are drawn in Section 5.

2. MODEL ESTABLISHMENT AND DYNAMIC CHARACTERISTIC TEST

2.1 System Description

The schematic diagram of the considered IES is illustrated in Fig. 1, which contains a micro gas turbine (MGT) unit, a PV module, a lithium battery and an air source heat pump (ASHP).

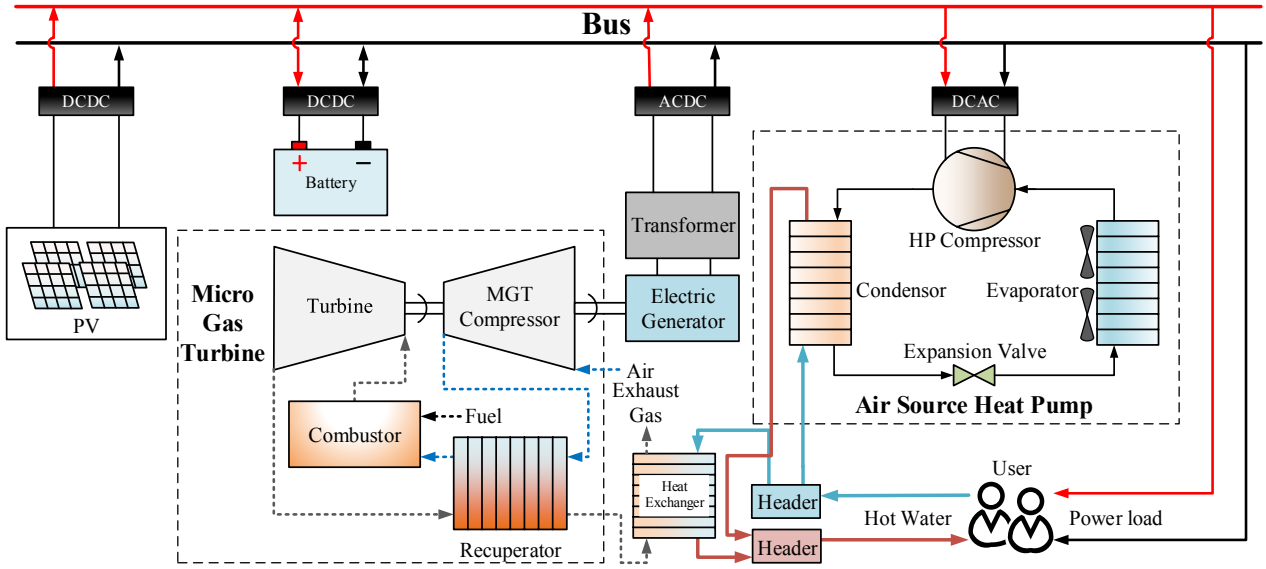

Fig. 1. The schematic diagram of the IES.

This system is intended to supply both electricity and heat for residential usage. The PV module absorbs solar energy and generates environment-friendly electricity. The MGT unit operates in CHP mode, supplying both reliable electricity and heat. The lithium battery plays a vital role to stabilize the grid voltage and store the energy.

In reaching the target of satisfying the electricity and heat demand simultaneously, a sole CHP mode MGT is not sufficient. There are two controlled variables, power and heat, while the MGT can only provide one degree of freedom in control. By introducing an ASHP into the system, a degree of freedom in control is added in thermal side. In this case, the heating and hot water demand is met by the MGT and the ASHP together.

The capacity allocation of the system is based on the energy efficiency and investment cost. According to a rational capacity proportion，the allocation is set as 80kW MGT, 60kW PV module and 60Ah battery. According to the thermal demand of users, the rated input power of the ASHP is 60kW. These sources and storage form a 380V DC micro grid. The single bus structure is applied for this system because of its relative low investment cost and simplicity.

2.2 The PV model

The theoretical model of the PV module is divided into three parts, the PV cell, the MPPT controller and the boost circuit.

The I-V characteristic of PV cell can be expressed as (Kneiske, et al., 2018).

$$I_{PV} = I_{ph} - I_d - I_{sh} = I_{ph} - I_0\left[e^{\frac{V+IR_s}{nkT_{cell}/q}} - 1\right] - \frac{V + I_{PV}R_s}{R_{sh}} \quad (1)$$

The perturb-and-observe method is adopted for PV maximum power point tracking (MPPT) in this paper.

2.3 Micro Gas Turbine Model

The MGT system consists of a centrifugal compressor, a radial turbine, a combustor and a recuperator. As the full-regenerative MGT introduced in this paper, all the compressed air is heated by the high temperature exhaust gas from the turbine. In view of the strong independence of the MGT components, modular modelling method is used (Zhang et al., 2010). The core formulas of each component are given as below.

The accurate performance of the compressor is usually obtained from experiment, which can be summarized into a set of equations (Zhang, 2015). The meaning of symbols is tabulated in the Appendix A.

$$\begin{aligned} T_{c2} &= T_{c1}\left[1 + \left(\pi_c^{k_a} - 1\right)/\eta_c\right] \\ N_c &= m_c c_{pa} T_{c1}\left(\pi_c^{k_a} - 1\right)/\eta_c \end{aligned} \quad (2)$$

The combustor outlet flow rate, temperature and pressure can be calculated as

$$\begin{aligned} m_{b1} &= (1-k_{cl})m_c, m_{b2} = m_{b1} + m_f \\ T_{b2} &= \left[m_{b1} c_{pa} T_{c2} + m_f \left(Q_{cv,f} \eta_b + i_f \right) \right] / c_{pg} m_{b2} \\ P_{b2} &= \varepsilon_b P_{b1} \end{aligned} \tag{3}$$

The modelling of the turbine depends on the reduced parameters π_t and η_t. Ignoring the heat exchange of the gas pipeline between the combustor and the turbine, the turbine inlet temperature can be regarded as the same as the combustor outlet temperature. Therefore, the outlet temperature and power of the turbine can be determined by

$$\begin{aligned} T_{t1} &= T_{b2} \\ T_{t2} &= T_{t1} \left[1 - \left(1 - 1/\pi_t^{k_g} \right) \eta_t \right] \\ N_t &= m_t c_{pa} T_{t1} \left(1 - 1/\pi_t^{k_g} \right) \eta_t \end{aligned} \tag{4}$$

The mainstream type of the recuperator for a MGT system is main surface heat transfer because of its high heat transfer efficiency and compactness. The heat transfer process of the exhaust gas and the air can be defined as

$$\begin{cases} \dfrac{\partial \left(\rho_a A_a c_{pa} T_a \right)}{\partial t} + \dfrac{\partial \left(m_a c_{pa} T_a \right)}{\partial x} + \alpha_a A_a \left(T_a - T_j \right) = 0 \\ \dfrac{\partial \left(\rho_g A_g c_{pg} T_g \right)}{\partial t} + \dfrac{\partial \left(m_g c_{pg} T_g \right)}{\partial x} + \alpha_g A_g \left(T_g - T_j \right) = 0 \\ \rho_j c_{pj} A_j \dfrac{\partial T_j}{\partial \tau} + \alpha_g A_g \left(T_g - T_j \right) + \alpha_a A_a \left(T_a - T_j \right) = 0 \end{cases} \tag{5}$$

The dynamic model of the rotor is obtained as

$$\begin{aligned} J\omega \frac{d\omega}{d\tau} &= N_t - N_c - N_{fr} - N_e \\ N_e &= N_{ed} \left(n / n_d \right)^2 \end{aligned} \tag{6}$$

A heat exchanger is used to utilize the waste heat of the exhaust gas. By assuming the temperature of the feed water remaining invariable, the heat transfer function is given as

$$\begin{aligned} \phi &= m_g c_{pg} \left(T_{g1} - T_{g2} \right) = m_a c_{pa} \left(T_{a2} - T_{a1} \right) \\ \phi &= \alpha A \left[(T_{g1} - t_{a2}) - (T_{g2} - t_{a1}) \right] / \ln \frac{T_{g1} - t_{a2}}{T_{g2} - t_{a1}} \end{aligned} \tag{7}$$

2.4 Lithium Battery Model

The commonly used lithium battery models include mathematical models, electrochemical models and electrical equivalent circuit network models. This paper mainly focuses on the internal charge-discharge process and the characteristics between the current and voltage, ignoring the physicochemical mechanism (Fotouhi et al., 2016).

In order to balance the energy supply and demand rapidly, the battery switches quickly between charging and discharging state. Thus, a bi-directional DC/DC converter is utilized to connect the battery to the grid. When the power supply and demand is unbalance, the battery will operate immediately to smooth the bus voltage within a second, avoid abnormal operation of the other loads caused by bus voltage fluctuation.

2.5 Air Source Heat Pump Model

The main components of an ASHP system include the compressor, condenser, evaporator and expanding valve. Due to the independence of each component, the theoretical model of the ASHP will be given in modular. For simplicity, lumped parameter method is adopted for temperature modelling (Wu et al., 2014).

Assuming the medium flow rate of the evaporator is the same as the one in compressor and ignoring the pressure and heat loss during evaporation, the thermal balance equation of the evaporator can be established according to the law of energy conservation.

$$\begin{aligned} \frac{1}{2} M_{w,ev} c_{pw} \frac{dt_{w1,ev} + dt_{w2,ev}}{d\tau} &= m_{ev} c_{pw} \left(t_{w1,ev} - t_{w2,ev} \right) - Q_{ev} \\ M_{r,ev} \frac{dh_{r,ev}}{d\tau} &= Q_{r,ev} - m_{r,ev} \left(h_1 - h_4 \right) \\ Q_{ev} &= \alpha_{ev} A_{ev} \left[\left(t_{w1,ev} + t_{w2,ev} \right) / 2 - t_{ev} \right] \end{aligned} \tag{8}$$

The compressor model is based on the performance test data of the specific compressor type. The vital variable representing the characteristic of the compressor is the pressure ratio of the condensing pressure and the evaporating pressure, which is denoted as $\varepsilon = p_{de}/p_{ev}$, while p_{de} and p_{ev} are determined by the temperature and the characteristic of the refrigerant. Thus, the compressor outlet refrigerant enthalpy and its power demand can be obtained as

$$\begin{aligned} m_r &= V_{cp} \omega_{cp} \eta_{v,cp} \lambda_{v,cp} / v_{r1} \\ h_2 &= h_1 + N / m_{r,cp} \\ N &= N_t / \eta_{e,eff} = \frac{n_{cp}}{1 - n_{cp}} \eta_v V_{cp} \omega_{cp} p_e \left[1 - \varepsilon^{(n_{cp}-1)/n_{cp}} \right] \end{aligned} \tag{9}$$

The operation process of condenser is actually as the inverse process as evaporator. Thus, the model can be expressed as

$$\begin{aligned} \frac{1}{2} M_{w,de} c_{pw} \frac{dt_{w1,de} + dt_{w2,de}}{d\tau} &= Q_{de} - m_{w,de} c_{pw} (t_{w2,de} - t_{w1,de}) \\ M_{r,de} \frac{dh_{r,de}}{d\tau} &= m_{r,de} (h_2 - h_1) - Q_{de} \\ Q_{de} &= \alpha_{de} A_{de} \left[t_{de} - (t_{w1,de} + t_{w2,de}) / 2 \right] \end{aligned} \tag{10}$$

Assuming the flow rate of the refrigerant remaining unchanged, the enthalpy value before and after flowing through the expanding valve is the same, namely, $h_3 = h_4$.

2.6 Header Model

The two paths hot water generated from the MGT and the ASHP are mixed in a header before delivering to domestic heating. The hot water temperature of the mixture is calculated as

$$Q = c_{pa} m_{hw,MGT}(t_{hw} - t_{hw,MGT}) = c_{pa} m_{hw,ASHP}(t_{hw,ASHP} - t_{hw})$$
$$t_{hw} = \frac{m_{hw,ASHP} t_{hw,HP} + m_{hw,MGT} t_{hw,MGT}}{m_{hw,ASHP} + m_{hw,MGT}} \quad (11)$$

3. PROBLEM FORMULATION AND CONTROL STRATEGY DESIGN

3.1 Overall System Dynamic Response

To provide prior accordance for the control design, the dynamic characteristics of the system should be given. Herein, the fuel flowrate of the MGT and the rotating speed of the ASHP are selected as manipulated variables, which effect both heat and electricity. The open-loop step responses of the power and hot water temperature under the change of fuel flowrate and rotating speed are depicted in Fig. 2.

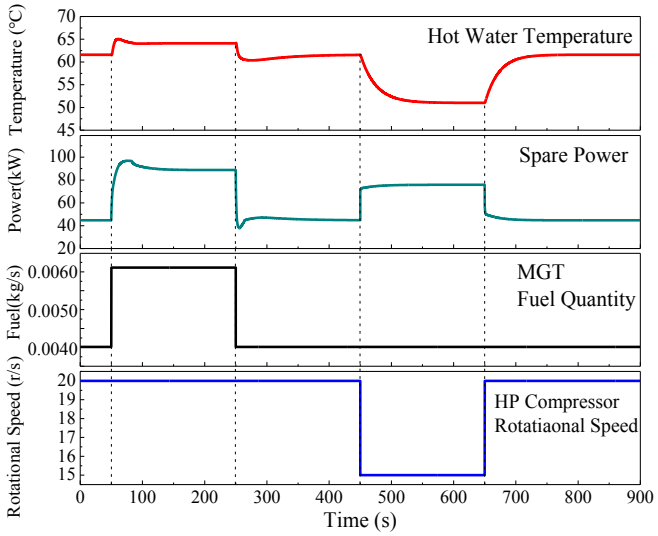

Fig. 2. The open-loop step response of the control system.

The fuel flowrate steps increase from 70% of the maximum to 100% at 50*s*, then decrease to the original value at 250*s*. The temperature of the hot water increases for 5℃ and spends 50 seconds for stabilization. The power supply increases for 45kW and the transition period is around 100 seconds. Although the steady-state values of the temperature and the power are equal to their original values after the fuel flowrate stepping downwards, the dynamic processes are different. It implies the nonlinearity of the MGT system, which brings in challenge to model based control strategy design.

The rotating speed of the HP compressor steps from 20*r/s* to 15*r/s* at 450*s* and recovers at 650*s*. The hot water temperature declines for 10℃ then recovers to the original value. The power firstly increases for 30kW and decreases to the previous value after the rotating speed stepping increase. The dynamic responses of the power and the temperature are quite different, while the former takes only 50 seconds to stabilize, the latter needs 100 seconds or even more. It clearly depicts the distinction between the electrical and thermal process.

3.2 Control System Description

The purpose of the proposed control strategy is to stabilize the bus voltage and the temperature of the hot water simultaneously under internal and external disturbances. The electricity is mainly supplied by the MGT and the PV module. The intermittent power generation of PV is processed as source-side disturbance. The domestic hot water is the mixture of the water heated by the MGT and the ASHP.

The difficulty of designing the control strategy derived from two aspects. On the one hand, because of the relatively large inertia of thermal objects, the dynamic response of the hot water temperature is much slower than the electrical ones. The distinction between these two kinds of objects may cause sluggish control performance or even divergence. Nevertheless, because the MGT is operating under CHP mode, and the power demand of the ASHP compressor is directly extracted from the stand-alone micro grid. The thermal and electricity generations are coupled, which also bring in challenges to controller design.

Based on the analyzation above, a centralized MPC controller is adopted to provide coordinated control of the MGT-CCHP and ASHP units, so that the thermal and electrical balance of the IES can be achieved.

The schematic diagram of the proposed control system is shown in Fig.3, where a two-input-two-output control system is proposed for the IES. The control variables are the fuel flowrate of the MGT, m_f and the rotating speed of the ASHP compressor, ω_c. The controlled variables are the spare power, N_s and the temperature of hot water, t_{hw}.

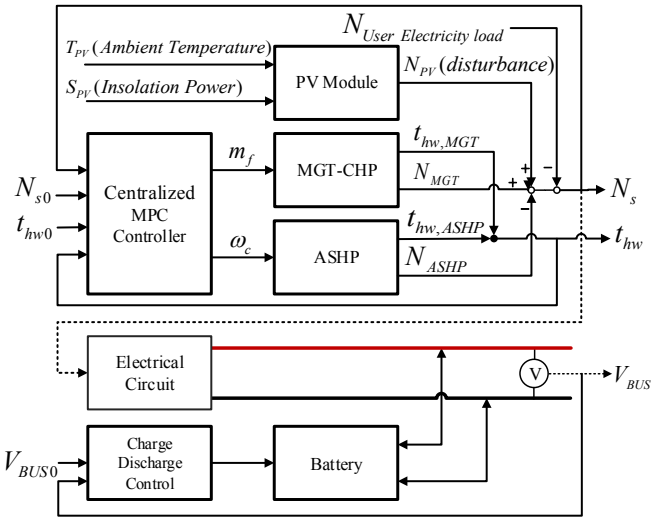

Fig. 3. MGT-PV-Battery-ASHP system control structure.

The spare power is the summation of power generated by the MGT and the PV module subtracting the power used by the ASHP and the electricity power required by users, which is denoted as

$$N_s = N_{MGT} + N_{PV} - N_{ASHP} - N_{User\ Electricity\ load} \tag{12}$$

where N_s is the spare power; N_{MGT} is the power generation of the MGT unit; N_{PV} is the power generation of the PV module. N_{ASHP} is the power demand of the ASHP compressor; $N_{User\ Electricity\ Load}$ is the electricity load power of users. The unit of all the parameters in (12) is *kW*.

The set-point of N_s is zero, corresponding to the exact electric power balance of the system. The temperature set-point is 60℃. The PV power generation and load demand are regarded as disturbances.

3.3 MPC Controller Design

The MPC controller is designed based on the discrete state space model of the MGT-HP system.

$$\begin{aligned} \boldsymbol{x}_d(k+1) &= \boldsymbol{A}_d \boldsymbol{x}_d(k) + \boldsymbol{B}_d \boldsymbol{u}(k) \\ \boldsymbol{y}(k) &= \boldsymbol{C}_d \boldsymbol{x}_d(k) \end{aligned} \tag{13}$$

In order to achieve zero offset, the integral embedded augmented model is developed for the further controller design.

$$\begin{aligned} \overbrace{\begin{bmatrix} \Delta \boldsymbol{x}_d(k+1) \\ \boldsymbol{y}(k+1) \end{bmatrix}}^{\boldsymbol{x}(k+1)} &= \overbrace{\begin{bmatrix} \boldsymbol{A}_d & \boldsymbol{O} \\ \boldsymbol{C}_d \boldsymbol{A}_d & \boldsymbol{I} \end{bmatrix}}^{\boldsymbol{A}} \overbrace{\begin{bmatrix} \Delta \boldsymbol{x}_d(k) \\ \boldsymbol{y}(k) \end{bmatrix}}^{\boldsymbol{x}(k)} + \overbrace{\begin{bmatrix} \boldsymbol{B}_d \\ \boldsymbol{C}_d \boldsymbol{B}_d \end{bmatrix}}^{\boldsymbol{B}} \Delta \boldsymbol{u}(k) \\ \boldsymbol{y}(k) &= \overbrace{\begin{bmatrix} \boldsymbol{O} & \boldsymbol{I} \end{bmatrix}}^{\boldsymbol{C}} \begin{bmatrix} \Delta \boldsymbol{x}_d(k) \\ \boldsymbol{y}(k) \end{bmatrix} \end{aligned} \tag{14}$$

The cost function and the constraints are given in (15).

$$\begin{aligned} \min\ & J = \left\| \boldsymbol{Y}_r - \boldsymbol{Y} \right\|_Q^2 + \left\| \Delta \boldsymbol{U} \right\|_R^2 \\ s.t.\ & \boldsymbol{u}_{\min} \le \boldsymbol{u} \le \boldsymbol{u}_{\max} \\ & \Delta \boldsymbol{u}_{\min} \le \Delta \boldsymbol{u} \le \Delta \boldsymbol{u}_{\max} \end{aligned} \tag{15}$$

4. CONTROL SIMULATION RESULTS

The control result is presented in Fig. 4, including the performance with source-side, load-side and thermal-side disturbances. The set-point of the bus voltage and hot water temperature is 380*V* and 60℃, respectively.

The system response under load-side disturbance is shown in the first section of Fig. 4. A 5kW DC impedance load joins the micro-grid at 50*s*. It shows that when the electricity supply is scarce, the battery will charge the grid immediately to balance the energy. The MGT fuel flowrate also increases rapidly to compensate the electricity deficiency, while the temperature of the exhaust gas increases. Thus, the rotating speed of the HP compressor drops to balance the hot water temperature, which also leads to the drop of the load demand. The total transient period of the process is around 50 seconds.

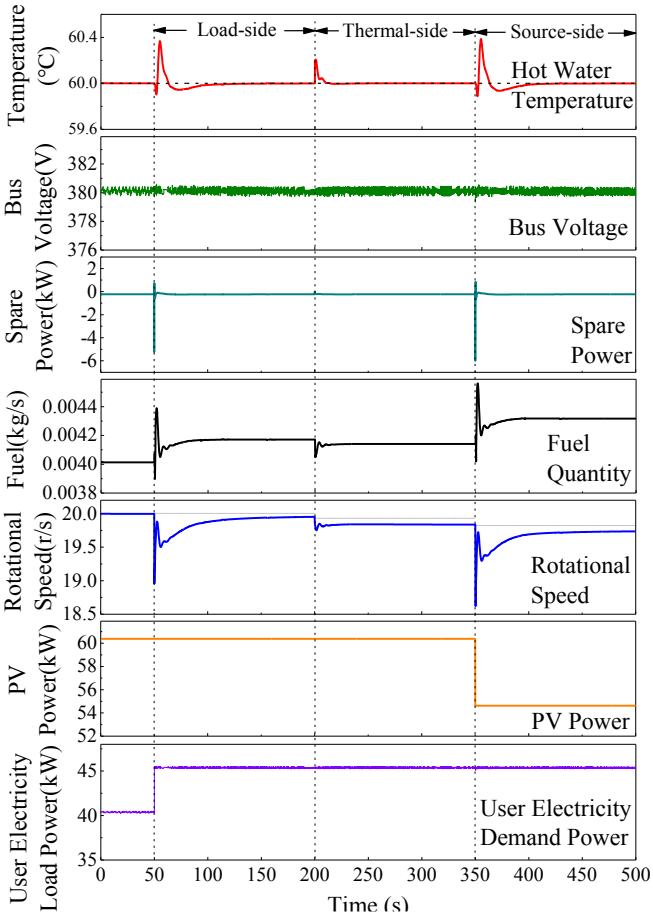

Fig. 4. The system response under load-side, thermal-side and source-side disturbances.

The second section depicts the system response under thermal-side disturbance, which reveals as the 0.2℃ increase at 200s due to the decrease of hot water flow rate of user-side. The fuel flowrate of MGT and the rotating speed of the HP compressor drops to reduce the temperature, leading to the change of the power balance. Thus, the grid voltage fluctuates slightly till the end of the adjustment process. And the hot water temperature also regresses within 20 seconds.

The third section of Fig. 4 represents the system response under source-side disturbance. At 350*s*, the insolation power of the PV pedal steps downwards from $2000 W/m^2$ to $1900 W/m^2$, which causes 6kW power drop. Thanks to the quick charging action of the battery, the grid voltage only fluctuates slightly. Meanwhile, the temperature of hot water recovers after 50 seconds with a small over shoot less than 0.3℃.

The simulation results show satisfactory control performance of the MPC controller under difference types of disturbances. The distinction between the dynamic characteristics of electrical and thermal processes can be effectively handled by the proposed control strategy. In summary, the MPC is suitable for the application in balancing the CHP micro grid energy.

5. CONCLUSION

The potential feasibility of MPC in coordinating both power and heat in stand-alone IES is validated. This paper first establishes a detailed theoretical model of a MGT/PV/Battery/ASHP hybrid IES. The systematic dynamic characteristic is simulated. It shows that the transient periods of thermal processes are much longer than the one of electrical processes, which brings in challenges to the simultaneously control of both objects. To conquer the problem, a centralized MPC is applied to coordinate the power and heat supply of the IES. The control simulation result shows that, even in the presence of disturbances from load, electrical and thermal sides, the control system can keep good balance between energy deliver and load demand.

The further research direction could be the economic optimization of the system. Economic index like the fuel cost, the state of charge of batteries should be taken into consideration. It will be reflected in the modification of systematic objective function. Keeping the stability of both power and thermal grid, while reaching the optimal economy, is the current study.

ACKNOWLEDGEMENT

This work was supported by National Natural Science Foundation of China under Grant 51936003, National Key R&D Program of China under Grant 2018YFB1502900 and the Royal Society - Sino British Fellowship Trust International Fellowship.

REFERENCES

Das, B. K., & Al-Abdeli, Y. M. (2017). Optimisation of stand-alone hybrid CHP systems meeting electric and heating loads. *Energy Conversion and Management*, 153, 391-408.

Fotouhi, A., Auger, D. J., Propp, K., Longo, S., & Wild, M. (2016). A review on electric vehicle battery modelling: From Lithium-ion toward Lithium–Sulphur. *Renewable and Sustainable Energy Reviews*, 56, 1008-1021.

Kneiske, T. M., Braun, M., & Hidalgo-Rodriguez, D. I. (2018). A new combined control algorithm for PV-CHP hybrid systems. *Applied Energy*, 210, 964-973.

Wu, W. , You, T. , Wang, B. , Shi, W. , & Li, X. . (2014). Simulation of a combined heating, cooling and domestic hot water system based on ground source absorption heat pump. *Applied Energy*, 126, 113-122.

Zhang, J., Shen, J., Ge, B., & Li, Y. (2010, March). Modeling and Dynamic Analysis of Adjustable Regenerative Microturbine. *In 2010 Asia-Pacific Power and Energy Engineering Conference* (pp. 1-4). IEEE.

Zhang, J. (2015). Integrated Optimization and Dynamic Characteristic Research On Microturbine-based Cooling, Heating and Power System. (Doctoral dissertation).

Zhang, Y., Meng, F., Wang, R., Kazemtabrizi, B., & Shi, J. (2019). Uncertainty-resistant stochastic MPC approach for optimal operation of CHP microgrid. *Energy*, 179, 1265-1278.

APPENDIX A. NOMENCLATURE

PV Module	
I_{ph}	photo current, A
I_d	current flowing through the diode, A
I_0	cell reverse saturation current, A
R_s	series resistance, Ω
R_{sh}	shunt resistance, Ω
T_{cell}	cell temperature, K
a	modified ideal factor
k	Boltzman constant, $1.38\times10^{-23} J/K$
n	diode ideal factor
q	electron charge, $1.6\times10^{-19} C$
Micro Gas Turbine and Air Source Heat Pump	
Variables	
T_1/T_2	inlet and outlet temperature, $°C$
P_1/P_2	Inlet and outlet flow pressure, kPa
A	heat transfer area, m^2
J	torque, $N{\cdot}m$
M	quantity, kg
N	power, kW
Q	heat capacity, kW
V	gas displacement, m^3
Q_{cv}	calorific value, kJ/kg
i	physical enthalpy, kJ/kg
h	enthalpy, kJ/kg
m	flow rate, kg/s
v	specific volume, m^3/kg
α	heat transfer coefficient, $W/(m^2{\cdot}K)$
ρ	density, kg/m^3
ϕ	heat exchange capacity, kW
ω	rotational speed, r/s
Parameters	
π/η	reduced parameters of specific compressors
c_p	specific heat capacity, $kJ/(kg{\cdot}°C)$
k_a	air adiabatic index
k_{cl}	air cooling coefficient
n	polytropic exponent
n_d	rated rotational speed of the turbine, m/s
η_v	volume efficiency
λ_v	volume coefficient
Subscript	
a	*air*
b	combustor
c	compressor
e	electrical
f	fuel
g	gas
j	metal wall
t	turbine
w	water
cp	compressor of heat pump
de	condenser
ed	rated
ev	evaporator
fr	mechanical friction loss
hw	hot water
re	refrigerant
eff	efficiency